ELSEVIER

Elastic Z^0 production at HERA

L. Stanco, on behalf of the ZEUS Collaboration

INFN–Padova, Via Marzolo, 8 I-35131 Padova, Italy

Abstract

The production of Z^0 bosons in the reaction $ep \rightarrow eZ^0p^{(*)}$, where $p^{(*)}$ stands for a proton or a low-mass nucleon resonance, has been studied in ep collisions at HERA using the ZEUS detector. The analysis is based on a data sample collected between 1996 and 2007, amounting to 496 pb^{-1} of integrated luminosity. The Z^0 was measured in the hadronic decay mode. The elasticity of the events was ensured by a cut on $\eta_{max} < 3.0$, where η_{max} is the maximum pseudorapidity of energy deposits in the calorimeter defined with respect to the proton beam direction. A signal was observed at the Z^0 mass. The cross section of the reaction $ep \rightarrow eZ^0p^{(*)}$ was measured to be $\sigma\left(ep \rightarrow eZ^0p^{(*)}\right) = 0.13 \pm 0.06\,(\text{stat.}) \pm 0.01\,(\text{syst.})$ pb, in agreement with the Standard Model prediction of 0.16 pb. This is the first measurement of Z^0 production in ep collisions. In this paper we report the already published ZEUS result by adding the sensitivities of the most recent similar results from CMS and ATLAS.

Keywords: e–p interactions, Z^0 boson

1. Introduction

The production of electroweak bosons in ep collisions is a good benchmark process for testing the Standard Model (SM). Even though the expected numbers of events for $W^\pm$ and Z^0 production are low, the measurement of the cross sections of these processes is important as some extensions of the SM predict anomalous couplings and thus changes in these cross sections. A measurement of the cross section for $W^\pm$ production at HERA has been performed by H1 and ZEUS [2] in events containing an isolated lepton and missing transverse momentum, giving a cross section $\sigma(ep \rightarrow W^\pm X) = 1.06 \pm 0.17\,(\text{stat.} \oplus \text{syst.})$ pb, in good agreement with the SM prediction. The cross section for Z^0 production is predicted to be 0.4 pb.

This paper reports on a measurement of the production of Z^0 bosons in $e^\pm p$ collisions using an integrated luminosity of about 0.5fb^{-1}. The hadronic decay mode was chosen[1] because of its large branching ratio. The

excellent resolution of the ZEUS hadronic calorimeter makes this measurement possible. The analysis was restricted to elastic and quasi-elastic Z^0 production in order to suppress QCD multi-jet background. The selected process is $ep \rightarrow eZ^0p^{(*)}$, where $p^{(*)}$ stands for a proton (elastic process) or a low-mass nucleon resonance (quasi-elastic process).

The corresponding and final result has been already published by the ZEUS Collaboration in [1] which content corresponds to this report with the addition of LHC comparison.

Fig. 1 shows a leading-order (LO) diagram of Z^0 production with subsequent hadronic decay. In such events, there are at least two hadronic jets with high transverse energies, and no hadronic energy deposits around the forward[2] direction, in contrast to what would be ex-

---

[1]The Z^0 decay into charged lepton pairs was studied in a previous ZEUS publication [3].

[2]The ZEUS coordinate system is a right-handed Cartesian system, with the Z axis pointing in the proton beam direction, referred to as the forward direction, and the X axis pointing towards the centre of HERA. The coordinate origin is at the nominal interaction point. The pseudorapidity is defined as $\eta = -\ln\left(\tan\frac{\theta}{2}\right)$, where the polar angle, θ, is measured with respect to the proton beam direction.
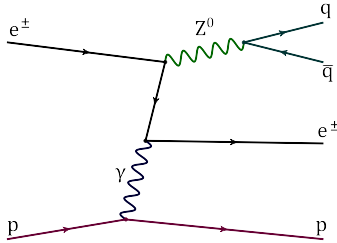
pected in inelastic collisions.

Figure 1: Example of a leading-order diagram of Z^0 boson production and subsequent hadronic decay (into quark q and antiquark $\bar{q}$) in $ep \rightarrow eZ^0p$.

2. Experimental set-up

HERA was the world's only high-energy ep collider, with an electron[3] beam of 27.6 GeV and a proton beam of 920 GeV (820 GeV until 1997). For this analysis, $e^{\pm}p$ collision data collected with the ZEUS detector between 1996 and 2007, amounting to 496 pb^{-1} of integrated luminosity, have been used. They consist of 289 pb^{-1} of e^+p data and 207 pb^{-1} of e^-p data.

After 2003, HERA was operated with a polarised lepton beam. When combining the data taken with negative and positive polarisations, the average polarisation is less than 1% and its effect was neglected in this analysis.

A detailed description of the ZEUS detector can be found elsewhere [3 in ref. 1]. A brief outline of the calorimeter that is most relevant for this analysis follows.

The high-resolution uranium–scintillator calorimeter (CAL) [4] consisted of three parts: the forward (FCAL), the barrel (BCAL) and the rear (RCAL) calorimeters. Each part was subdivided transversely into towers and longitudinally into one electromagnetic section (EMC) and either one (in RCAL) or two (in BCAL and FCAL) hadronic sections (HAC). The smallest subdivision of the calorimeter was called a cell. The CAL energy resolutions, as measured under test-beam conditions, were $\sigma(E)/E = 0.18/\sqrt{E}$ for electrons and $\sigma(E)/E = 0.35/\sqrt{E}$ for hadrons, with E in GeV.

The luminosity was measured using the Bethe–Heitler reaction $ep \rightarrow e\gamma p$. The fractional systematic uncertainty on the measured luminosity was 2%.

---

[3]The term "electron" also refers to positrons if not stated otherwise.

3. Monte Carlo simulations

Monte Carlo (MC) simulations were made to simulate the Z^0 production process. They were used to correct for instrumental effects and selection acceptance and to provide a template for the shape of the invariant-mass distribution of the Z^0 signal. The EPVEC program [5] was used to generate the signal events at the parton level. The following Z^0 production processes are considered in EPVEC:

- elastic scattering, $ep \rightarrow eZ^0p$, where the proton stays intact;
- quasi-elastic scattering, $ep \rightarrow eZ^0p^*$, where the proton is transformed into a nucleon resonance p^*;
- deep inelastic scattering (DIS), $\gamma^*p \rightarrow Z^0X$, in the region $Q^2 > 4\,\text{GeV}^2$, where Q^2 is the virtuality of the photon exchanged between the electron and proton;
- resolved photoproduction, $\gamma p \rightarrow \left(q\bar{q} \rightarrow Z^0\right)X$, where one of the quarks is a constituent of the resolved photon and the other quark is a constituent of the proton.

In EPVEC the first two processes are calculated using form factors and structure functions fitted directly to experimental data. Note that, even if the virtuality of the exchanged photon is small, the scattered electron could receive a large momentum transfer when the Z^0 is radiated from the lepton line. In the last two processes, the proton breaks up. The DIS process is calculated in the quark–parton model using a full set of leading-order Feynman diagrams. Resolved photoproduction is parametrised using a photon structure function and is carefully matched to the DIS region. The cross section of Z^0 production is calculated to be 0.16 pb for elastic and quasi-elastic processes and 0.24 pb for DIS and resolved photoproduction. The difference between e^+p and e^-p cross sections is negligible for this analysis (<1% for the DIS process). A correction, based on the MC cross section, was made to account for the part of data taken at the centre-of-mass energy $\sqrt{s} = 300$ GeV, so that the result is quoted at $\sqrt{s} = 318$ GeV.

After the parton-level generation by EPVEC, PYTHIA 5.6 [6] was used to simulate initial- and final-state parton showers with the fragmentation into hadrons using the Lund string model [7] as implemented in JETSET 7.3 [6]. The generated MC events were passed through the ZEUS detector and trigger simulation programs based on GEANT 3.13 [8]. They were reconstructed and analysed by the same programs as the data.

A reliable prediction of background events with the signal topology, which are predominantly due to the diffractive photoproduction of jets of high transverse momentum, is currently not available. Therefore, the background shape of the invariant-mass distribution was estimated with a data-driven method. The normalisation was determined by a fit to the data.

4. Event reconstruction and selection

The events used in this analysis were selected online by the ZEUS three-level trigger system [13 in ref. 1], using a combination of several trigger chains which were mainly based on requirements of large transverse energy deposited in the calorimeter. In the offline selection, further criteria were imposed in order to separate the signal from the background.

The events are characterised by the presence of at least two jets of high transverse energy and, for a fraction of events, by the presence of a reconstructed scattered electron. In order to select events with a Z^0 decaying hadronically, jets were reconstructed in the hadronic final state using the k_T cluster algorithm [9] in the longitudinally invariant inclusive mode [10]. The algorithm was applied to the energy clusters in the CAL after excluding those associated with the scattered-electron candidate [11, 12, 13]. Energy corrections [19–21 in ref. 1] were applied to the jets in order to compensate for energy losses in the inactive material in front of the CAL.

In this analysis, only jets with $E_T > 4\,\mathrm{GeV}$ and $|\eta| < 2.0$ were used. Here E_T is the jet transverse energy and η its pseudorapidity. The hadronic Z^0 decay sample was selected by the following requirements on the reconstructed jets:

- at least two jets in the event had to satisfy $E_T > 25\,\mathrm{GeV}$;
- $\left|\Delta\phi_j\right| > 2\,\mathrm{rad}$, where $\Delta\phi_j$ is the azimuthal difference between the first and second highest-E_T jet, as the two leading jets from the Z^0 boson decays are expected to be nearly back-to-back in the X–Y plane.

Electrons were reconstructed using an algorithm that combined information from clusters of energy deposits in the CAL and from tracks [11]. To be defined as well-reconstructed electrons, the candidates were required to satisfy the following selection:

- $E'_e > 5\,\mathrm{GeV}$ and $E_{\mathrm{in}} < 3\,\mathrm{GeV}$, where E'_e is the scattered electron energy and E_{in} is the total energy in all CAL cells not associated with the cluster of the electron but lying within a cone in η and

ϕ of radius $R = \sqrt{\Delta\eta^2 + \Delta\phi^2} = 0.8$, centred on the cluster;
- If the electron was in the acceptance region of the tracking system, a matched track was required with momentum $p_{\mathrm{track}} > 3\,\mathrm{GeV}$. After extrapolating the track to the CAL surface, its distance of closest approach (DCA) to the electron cluster had to be within 10 cm.

The following cuts were applied to suppress low-Q^2 neutral-current and direct-photoproduction backgrounds:

- $E_{\mathrm{RCAL}} < 2\,\mathrm{GeV}$, where E_{RCAL} is the total energy deposit in RCAL;
- $50 < E - p_Z < 64\,\mathrm{GeV}$, where $E - p_Z = \sum_i E_i\,(1 - \cos\theta_i)$; E_i is the energy of the i-th CAL cell, θ_i is its polar angle and the sum runs over all cells[4];
- $\theta_e < 80°$ for well reconstructed electrons, where θ_e is the polar angle of the scattered electron, motivated by the fact that, due to the large mass of the produced system, the electron is backscattered to the forward calorimeter or forward beam pipe;
- the event was rejected if more than one electron candidate was found;
- jets were regarded as a misidentified electron or photon and were discarded from the list of jets if the direction of the jet candidate was matched within $R < 1.0$ with that of an electron candidate identified by looser criteria[5] than those described above. This cut causes a loss of acceptance of about 3%.

To remove cosmic and beam–gas backgrounds, events fulfilling any of the conditions listed below were rejected:

- $|Z_{\mathrm{vtx}}| > 50\,\mathrm{cm}$, where Z_{vtx} is the Z position of the primary vertex reconstructed from CTD+MVD tracks;
- $175° < \left(\theta_{\mathrm{jet1}} + \theta_{\mathrm{jet2}}\right) < 185°$ and $\Delta\phi_j > 175°$ simultaneously, where θ_{jet1} and θ_{jet2} are the polar angles of the first and second highest-E_T jet, respectively, and $\Delta\phi_j$ is the azimuthal difference between them;
- $|t_u - t_d| > 6.0\,\mathrm{ns}$, where $|t_u - t_d|$ is the timing difference between the upper and the lower halves of the BCAL;

---

[4]For fully contained events, or events in which the particles escape only in the forward beam pipe, the $E - p_Z$ value peaks around twice the electron beam energy, 55 GeV.

[5] Candidates were selected by less stringent requirements and clusters with no tracks were also accepted to find photons and electrons.

- $\not{p}_T > 25\,\text{GeV}$, where $\not{p}_T$ is the missing transverse momentum calculated from the energy clusters in the CAL;
- $N_{\text{trk}}^{\text{vtx}} < 0.25\left(N_{\text{trk}}^{\text{all}} - 20\right)$, where $N_{\text{trk}}^{\text{vtx}}$ is the number of tracks associated with the primary vertex and $N_{\text{trk}}^{\text{all}}$ is the total number of tracks [14].

The number of events passing the above selection was 5257. Finally, to select the elastic and quasi-elastic processes preferentially, a cut on η_{max} was introduced,

- $\eta_{\text{max}} < 3.0$.

The quantity η_{max} was defined as the pseudorapidity of the energy deposit in the calorimeter closest to the proton beam direction with energy greater than $400\,\text{MeV}$ as determined by calorimeter cells. This cut also rejected signal events which have energy deposits from the scattered electron in the calorimeter around the forward beam pipe, causing an acceptance loss of about 30%.

After all selection cuts, 54 events remained. The total selection efficiency was estimated by the MC simulation to be 22% for elastic and quasi-elastic processes and less than 1% for DIS and resolved photoproduction events. The number of expected signal events in the final sample, as predicted by EPVEC, is 18.3. The contribution from elastic and quasi-elastic processes amounts to 17.9 events.

5. Background-shape study

Fig. 2(a) shows the distribution of the invariant mass, M_{jets}, after all the selection criteria except for the requirement $\eta_{\text{max}} < 3.0$. The variable M_{jets} was calculated using all jets passing the selection criteria described in Section 4. Figs. 2(b)-(d) show M_{jets} for various η_{max} slices in the inelastic region ($\eta_{\text{max}} > 3.0$) for the same selection. No significant dependence on η_{max} of the M_{jets} distribution beyond that expected from statistical fluctuations was observed in the inelastic region. In addition, the shape of the M_{jets} distribution outside the Z^0 mass window in the region $\eta_{\text{max}} < 3.0$ was found to be consistent with that in the inelastic region (Fig. 3). Therefore, the M_{jets} distribution in the inelastic region was adopted as a background template in a fit to the data in the elastic region as described in the following section.

6. Cross-section extraction

A fit to the sum of the signal and a background template for the M_{jets} distribution was used for the cross-
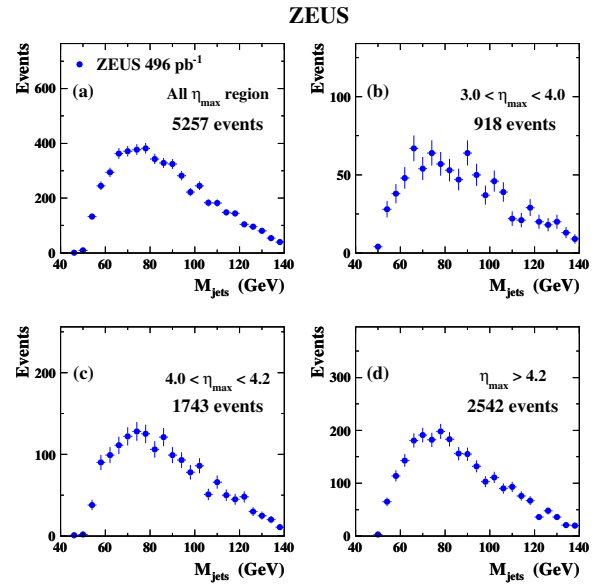
Figure 2: The M_{jets} distribution of the data (a) after all selection criteria, except for the η_{max} cut, (b-d) in several η_{max} slices.
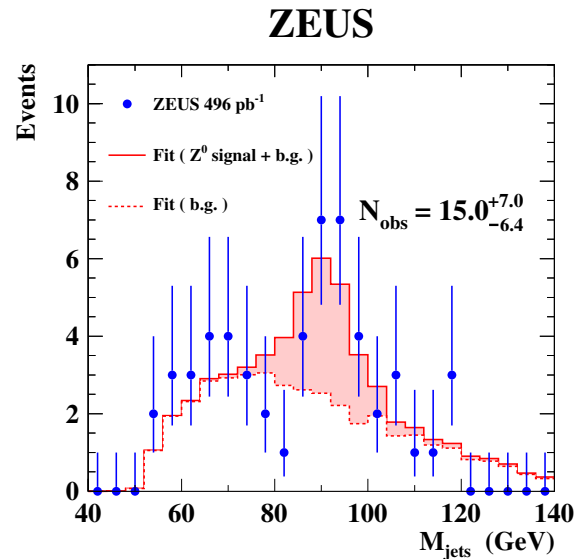
Figure 3: The M_{jets} distribution and the fit result. The data are shown as points, and the fitting result of signal+background (background component) is shown as solid (dashed) line. The signal contribution is also indicated by the shaded area and amounts to a total number of N_{obs} events. The error bars represent the approximate Poissonian 68% CL intervals, calculated as $\pm \sqrt{n + 0.25} + 0.5$ for a given entry n.

section extraction. The template $N_{\mathrm{ref},i}$ is defined according to:

$$N_{\mathrm{ref},i} = aN_{\mathrm{sg},i}^{\mathrm{MC}}(\epsilon) + bN_{\mathrm{bg},i}^{\mathrm{data}}, \qquad (1)$$

where i is the bin number of the M_{jets} distribution. The parameter ϵ accounts for a possible energy shift, i.e. $M_{\mathrm{jets}} = (1 + \epsilon) M_{\mathrm{jets}}^{\mathrm{MC}}$, where $M_{\mathrm{jets}}^{\mathrm{MC}}$ is the invariant-mass distribution of the signal Z^0 MC. The quantity $N_{\mathrm{sg},i}^{\mathrm{MC}}$ is a signal template estimated from the Z^0 MC distribution after all cuts, normalised to data luminosity. The quantity $N_{\mathrm{bg},i}^{\mathrm{data}}$ is a background template determined from the data outside the selected region. The parameters a and b are the normalisation factors for the signal and background, respectively. The likelihood of the fit, $\mathcal{L}$, is defined as follows:

$$\mathcal{L} = \mathcal{L}_1(N_{\mathrm{obs}}, N_{\mathrm{ref}}) \times \mathcal{L}_2(\epsilon, \sigma_\epsilon), \qquad (2)$$

with

$$\mathcal{L}_1 = \prod_i \frac{\exp(-N_{\mathrm{ref},i})(N_{\mathrm{ref},i})^{N_{\mathrm{obs},i}}}{N_{\mathrm{obs},i}!} \quad \text{and} \quad \mathcal{L}_2 = \exp\left(-\frac{\epsilon^2}{2\sigma_\epsilon^2}\right).$$

Here $\mathcal{L}_1(N_{\mathrm{obs}}, N_{\mathrm{ref}})$ is the product of Poisson probabilities to observe $N_{\mathrm{obs},i}$ events for the bin i when $N_{\mathrm{ref},i}$ is expected. The term $\mathcal{L}_2(\epsilon, \sigma_\epsilon)$ represents the Gaussian probability density for a shift ϵ of the jet energy scale from the nominal scale, which has a known systematic uncertainty of $\sigma_\epsilon = 3\%$. From the likelihood, a chi-squared function is defined as

$$\tilde{\chi}^2 = -2\ln\frac{\mathcal{L}_1(N_{\mathrm{obs}}, N_{\mathrm{ref}})}{\mathcal{L}_1(N_{\mathrm{obs}}, N_{\mathrm{obs}})} - 2\ln\mathcal{L}_2 = 2\sum f_i + \left(\frac{\epsilon}{\sigma_\epsilon}\right)^2, (3)$$

with

$$f_i = \begin{cases} N_{\mathrm{ref},i} - N_{\mathrm{obs},i} + N_{\mathrm{obs},i}\ln(N_{\mathrm{obs},i}/N_{\mathrm{ref},i}) & (\text{if } N_{\mathrm{obs},i} > 0) \\ N_{\mathrm{ref},i} & (\text{if } N_{\mathrm{obs},i} = 0). \end{cases}$$

The best combination of (a,b,ϵ) is found by minimising $\tilde{\chi}^2$. The value of a after this optimisation gives the ratio between the observed and expected cross section, i.e. $\sigma_{\mathrm{obs}} = a\sigma_{\mathrm{SM}}$. The maximum and minimum values of a in the interval $\Delta\tilde{\chi}^2 < 1$ define the range of statistical uncertainty.

7. Systematic uncertainties

Several sources of systematic uncertainties were considered and their impact on the measurement estimated.

- An uncertainty of 3% was assigned to the energy scale of the jets and the effect on the acceptance correction was estimated using the signal MC. The uncertainty on the Z^0 cross-section measurement was estimated to be +2.1% and −1.7%.

- The uncertainty associated with the elastic and quasi-elastic selection was considered. In a control sample of diffractive DIS candidate events, the $\eta_{\max}$ distribution of the MC agreed with the data to within a shift of $\eta_{\max}$ of 0.2 units [15]. Thus, the $\eta_{\max}$ threshold was changed in the signal MC by ±0.2, and variations of the acceptance were calculated accordingly. The uncertainty on the cross-section measurement was +6.4% and −5.4%.

- The background shape uncertainty was estimated by using different slices of $\eta_{\max}$ in the fit. The background shape was obtained using only the regions of $4.0 < \eta_{\max} < 4.2$ or $4.2 < \eta_{\max}$. The region of $3.0 < \eta_{\max} < 4.0$ was not used since a small number of signal events is expected in this $\eta_{\max}$ region[6]. The resulting uncertainty in the cross-section measurement was ±1.5%.

- The uncertainty associated with the luminosity measurement was estimated to be 2%, as described in Section 2.

- The Z^0 mass distribution from the MC used as a signal template has a Gaussian core width of 6 GeV. A possible systematic uncertainty coming from the width of the MC signal peak was studied. The mass fit was repeated after smearing the Z^0 mass distribution in the MC by a Gaussian function with different widths. The measured cross section did not change significantly after smearing the distribution up to the point where the fit $\tilde{\chi}^2$ changed by 1. No systematic uncertainty from this source was assigned.

The total systematic uncertainty was calculated by summing the individual uncertainties in quadrature and amounts to +7.2% and −6.2%.

8. Results and conclusions

Fig. 3 shows the invariant-mass distribution of the selected events. It also shows the fit result for the signal plus background and the background separately. As described in the previous sections, the background is mainly from diffractive multi-jet production, and the template of its invariant-mass distribution is determined from the data. The fit yielded a result for the parameter a from Eq. 1 of $a = 0.82^{+0.38}_{-0.35}$. That translates into a number of observed Z^0 events of $15.0^{+7.0}_{-6.4}$ (stat.), which corresponds to a signal with a 2.3σ statistical significance.

---

[6]The ratio of the expected number of signal MC events to the observed data in this region was estimated to be 2.6% for $80 < M_{\mathrm{jets}} < 100\,\mathrm{GeV}$, while in the other slices it was less than 0.4%.

The fit yielded a value for ϵ, the potential energy shift with respect to the signal MC, of $0.028^{+0.021}_{-0.020}$, which is compatible with zero. The correlation between the parameters a and ϵ is rather weak; when fixing the value of ϵ to zero the minimum $\tilde{\chi}^2$ is observed at $a = 0.65$. The quality was evaluated according to Eq. 3; the value of $\tilde{\chi}^2/\mathrm{ndf} = 17.6/22$, where ndf is the number of degrees of freedom, indicates a good fit. The cross section for the elastic and quasi-elastic production of Z^0 bosons, $ep \rightarrow eZ^0 p^{(*)}$, at $\sqrt{s} = 318\,\mathrm{GeV}$, was calculated to be

$$\sigma(ep \rightarrow eZ^0 p^{(*)}) = 0.13 \pm 0.06\,(\text{stat.}) \pm 0.01\,(\text{syst.})\,\text{pb}.$$

This result is consistent with the SM cross section calculated with EPVEC of 0.16 pb. This represents the first observation of Z^0 production in ep collisions.

9. Hadronic Z^0 mass resolutions at LHC

The excellent resolution obtained for the jet mass at the Z^0 scale is the best achieved so far in similar apparata. That is due to the excellent performances of the ZEUS hadronic calorimeter. By comparison we report the recent achievements from ATLAS and CMS experiments. For example, the result by ATLAS for the mass resolution obtained in $Z^0 \rightarrow b\bar{b}$ [16] is shown in Fig. 4. Similarly, in the CMS experiment the expected resolution on the di–jet mass scale is shown in Fig. 5 for the $H \rightarrow b\bar{b}$ decay [17]. In either case the resolution comes about a factor two worse than that obtained by the ZEUS calorimeter.
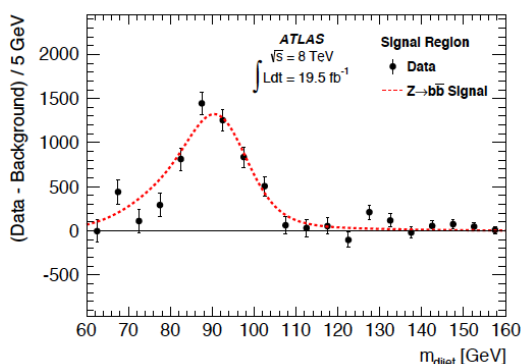

Figure 4: The ATLAS di–jet mass distribution of the selected events for $Z^0 \rightarrow b\bar{b}$ [16] search.
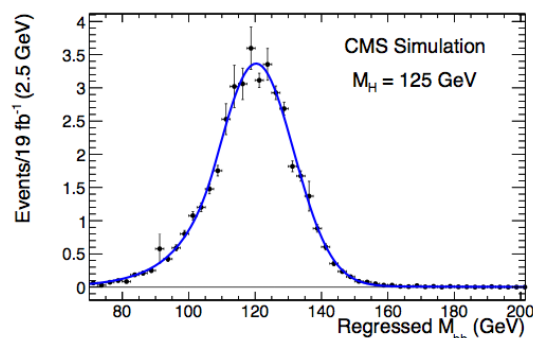
Acknowledgements

Figure 5: The CMS di–jet mass template for the event selection of $H \rightarrow b\bar{b}$ [17] (courtesy of the CMS Collaboration).

References

[1] ZEUS Collaboration, H. Abramowicz et a., Phys. Lett. B 718 (2013) 915, and references therein.
[2] H1 and ZEUS Coll., F.D. Aaron et al., JHEP, 1003 (2005) 035.
[3] S. Chekanov et.al., Phys. Lett. 680 (2009) 13.
[4] M. Derrick, et al., Nucl. Inst. Meth. A 309 (1991) 77;
A. Andresen, et al., Nucl. Inst. Meth. A 309 (1991) 101;
A. Caldwell, et al., Nucl. Inst. Meth. A 321 (1992) 356;
A. Bernstein, et al., Nucl. Inst. Meth. A 336 (1993) 23. M. Helbich, et al., Nucl. Inst. Meth. A 565 (2006) 572.
[5] U. Baur, J.A.M. Vermaseren, D. Zeppenfeld, Nucl. Phys. B 375 (1992) 3.
[6] T. Sjstrand, PYTHIA 5.6 and JETSET 7.3 physics and manual, CERN-TH.6488/92, 1992.
[7] B. Andersson, et al., Phys. Rep. 97 (1983) 31.
[8] R. Brun, et al., geant3, Tech. report CERN-DD/EE/84-1, 1987.
[9] S. Catani, et al., Nucl. Phys. B 406 (1993) 187.
[10] S.D. Ellis, D.E. Soper, Phys. Rev. D 48 (1993) 3160.
[11] ZEUS Coll., J. Breitweg, et al., Eur. Phys. J. C 11 (1999) 427.
[12] G.M. Briskin, Ph.D. Thesis, Tel Aviv University, 1998, Report DESY-THESIS 1998-036, available on http://www-library.desy.de/preparch/desy/thesis/desy-thesis-98-036.pdf.
[13] L.L. Wai, Preprint UMI-96-06968, 1995.
[14] ZEUS Coll., S. Chekanov, et al.,Phys. Lett. B 539 (2002) 197; ZEUS Collaboration, S. Chekanov, et al.,Phys. Lett. B 552 (2003) 308, Erratum.
[15] V. Sola, Ph.D. Thesis, Turin University, Report DESY-THESIS-2012-008, 2012, available on http://www-library.desy.de/preparch/desy/thesis/desy-thesis-12- 008.pdf.
[16] ATLAS Collaboration, arXiv:1404.7042.
[17] CMS Collaboration, arXiv:1403.3047, and CMS–PAS HIG-13–011 Archive Id: 184550P (courtesy of the CMS Collaboration).